Effects of volume mismatch and electronic structure on the decomposition of ScAlN and TiAlN solid solutions

Carina Höglund,[1] Björn Alling,[2] Jens Birch,[1] Manfred Beckers,[1] Per O. Å. Persson,[1] Carsten Baehtz,[3] Zsolt Czigány,[4] Jens Jensen,[1] and Lars Hultman[1]

[1]*Thin Film Physics Division, Department of Physics, Chemistry and Biology (IFM), Linköping University, SE-581 83 Linköping, Sweden*

[2]*Theory and Modeling Division, Department of Physics, Chemistry and Biology (IFM), Linköping University, SE-581 83 Linköping, Sweden*

[3]*Structural Diagnostics Division, Institute of Ion Beam Physics and Materials Research, Forschungszentrum Dresden-Rossendorf e.V., P.O. Box 510119, DE-01314 Dresden, Germany*

[4]*Research Institute for Technical Physics and Materials Science, Hungarian Academy of Sciences, P.O. Box 49, HU-1525 Budapest, Hungary*

(Received 16 March 2010; published 2 June 2010)

Thin solid films of metastable rocksalt structure (c-) $Sc_{1-x}Al_xN$ and $Ti_{1-x}Al_xN$ were employed as model systems to investigate the relative influence of volume mismatch and electronic structure driving forces for phase separation. Reactive dual magnetron sputtering was used to deposit stoichiometric $Sc_{0.57}Al_{0.43}N(111)$ and $Ti_{0.51}Al_{0.49}N(111)$ thin films, at 675 °C and 600 °C, respectively, followed by stepwise annealing to a maximum temperature of 1100 °C. Phase transformations during growth and annealing were followed *in situ* using x-ray scattering. The results show that the as-deposited $Sc_{0.57}Al_{0.43}N$ films phase separate at 1000–1100 °C into nonisostructural c-ScN and wurtzite structure (w-) AlN, via nucleation and growth at domain boundaries. $Ti_{0.51}Al_{0.49}N$, however, exhibits spinodal decomposition into isostructural coherent c-TiN and c-AlN, in the temperature interval of 800–1000 °C. X-ray pole figures show the coherency between c-ScN and w-AlN, with $AlN(0001)\|ScN(001)$ and $AlN\langle 0\bar{1}10\rangle\|ScN\langle\bar{1}10\rangle$. First-principles calculations of mixing energy-lattice spacing curves explain the results on a fundamental physics level and open a route for design of novel metastable pseudobinary phases for hard coatings and electronic materials.

DOI: 10.1103/PhysRevB.81.224101 PACS number(s): 64.75.−g, 81.40.−z, 81.15.−z, 81.30.−t

I. INTRODUCTION

Many transition-metal (TM) nitrides, e.g., TiN and CrN, form pseudobinary alloys with AlN in rocksalt structure (c-) $TM_{1-x}Al_xN$. These alloys are extensively used to increase the lifetime and cutting speed of coated tools[1–3] and $Ti_{1-x}Al_xN$ is by far the most explored system within this field. It is superior to TiN, which oxidizes rapidly above 550 °C leading to deteriorated mechanical properties. $Ti_{1-x}Al_xN$, however, has an excellent oxidation resistance up to above 700 °C (Ref. 4) due to a protective Al-rich oxide layer forming on the film surface.[5] It has also been shown that $Ti_{1-x}Al_xN$ coatings improve the cutting performance due to an age-hardening mechanism at high temperatures.[6]

This age hardening has been explained by a spinodal decomposition process in which the metastable $Ti_{1-x}Al_xN$ solid solution decomposes into coherent isostructural c-TiN and metastable c-AlN without a nucleation barrier. When the metastable $Ti_{1-x}Al_xN$ phase is annealed, kinetic barriers for diffusion are overcome and spontaneous compositional fluctuations appear. The local fluctuations evolve into modulations that do not break the coherency of the lattice but instead induce considerable strain leading to age hardening.[7–9] This mechanism counteracts the normal lattice softening caused by defect annihilation seen in, e.g., pure TiN films.[10] The spinodal decomposition of $Ti_{1-x}Al_xN$ is by now well established,[6,11,12] where the material decomposes at a temperature of ~1000 °C. At a temperature of 1400 °C, the decomposition process is completed by the formation of the equilibrium phases c-TiN and w-AlN, leading to a decreased hardness.[6] Theoretical studies have shown that the driving force for phase separation in $Ti_{1-x}Al_xN$, manifested by a positive isostructural mixing enthalpy, is mainly due to an electron band-structure effect. This effect is more pronounced for AlN concentrations above 50%.[13]

Sc-Al-N is in contrast to Ti-Al-N still a relatively unexplored material system, with the inverse perovskite Sc_3AlN being the only reported ternary compound.[14,15] Recently we found that AlN molar fractions of up to 60% can be dissolved into c-$Sc_{1-x}Al_xN(111)$,[16] which is similar to the metastable solubility of ~60% AlN in c-$Ti_{1-x}Al_xN$ for magnetron sputtered thin films.[3,17,18] First-principles calculations show that the magnitude of the isostructural cubic mixing enthalpy of $Sc_{1-x}Al_xN$ is very similar as for $Ti_{1-x}Al_xN$.[19,20] Unlike $Ti_{1-x}Al_xN$, there is no electronic band-structure driving force for decomposition in $Sc_{1-x}Al_xN$ but instead there is a large volume mismatch inducing a positive mixing enthalpy. Like in $Ti_{1-x}Al_xN$, though, higher AlN contents yield a mixed system including w-$Sc_{1-x}Al_xN$.[16]

In this work, we performed experiments of the thermal stability and decomposition mechanism during annealing of metastable c-$Sc_{0.57}Al_{0.43}N$ and c-$Ti_{0.51}Al_{0.49}N$ films. The compositions of the respective systems were chosen to be similar and close to the center of its miscibility gap but slightly low in AlN content to ensure that the solid solution grows single phase to suppress any surface-initiated phase separation. We reveal differences in patterns and mechanisms for decompositions of the two systems, caused by the different origins of decomposition driving forces present in $TM_{1-x}Al_xN$ pseudobinaries. *In situ* x-ray diffraction (XRD)

was used to follow the growth of epitaxial $Sc_{0.57}Al_{0.43}N(111)$ and $Ti_{0.51}Al_{0.49}N(111)$ thin films by magnetron sputtering and their development during subsequent annealing. *Ex situ* characterization was performed with analytical transmission electron microscopy and ion-beam analysis. The topotaxial relations between the end products were determined by pole figures measured by x-ray diffraction.

II. EXPERIMENTAL PROCEDURES

The experiments were performed in a high-vacuum sputter deposition chamber equipped with Be windows,[21] mounted onto the goniometer of the ROBL beamline (BM20) operated by the Forschungszentrum Dresden-Rossendorf, Germany, at the European Synchrotron Radiation Facility, Grenoble. The setup enables *in situ* x-ray scattering measurements during film growth and postdeposition annealing at a base pressure of $\sim 5 \times 10^{-4}$ Pa. Reactive dual magnetron sputtering with two 25 mm diameter Sc (or Ti) and Al targets was used to grow epitaxial and rocksalt-structure $Sc_{0.57}Al_{0.43}N$ and $Ti_{0.51}Al_{0.49}N$ films onto polished single-crystal substrates, $10 \times 10 \times 0.5$ mm^3 in size. Approximately 120-nm-thick $Sc_{0.57}Al_{0.43}N$ films were deposited onto ~60 nm ScN(111) seed layers on MgO(111) substrates while ~220-nm-thick $Ti_{0.51}Al_{0.49}N$ films were deposited onto $Al_2O_3(0001)$ substrates without seed layers.

The substrates were cleaned in ultrasonic baths of acetone and 2-propanol and blown dry in He. This was followed by degassing for 1 h at 1000 °C for MgO and 600 °C for Al_2O_3, respectively. The substrate temperatures were 600 °C for ScN and $Ti_{0.51}Al_{0.49}N$ and 675 °C for $Sc_{0.57}Al_{0.43}N$. The temperatures were controlled by a *K*-type thermocouple, and the required temperatures for isostructural decomposition of c-$Ti_{1-x}Al_xN$ are comparable with earlier reported values.[6,12] The dc magnetron powers were set to $P_{Sc}=56$ W for ScN, to $P_{Sc}=56$ W and $P_{Al}=28$ W for $Sc_{0.57}Al_{0.43}N$, and to $P_{Ti}=54$ W and $P_{Al}=26$ W for $Ti_{0.51}Al_{0.49}N$. The substrate bias was set to −30 V. The N_2/Ar fluxes, measured in standard cubic centimeter per minute, were initially set to 0.6/4.46 for ScN, 0.8/4.44 for $Sc_{0.57}Al_{0.43}N$, and 0.87/4.44 for $Ti_{0.51}Al_{0.49}N$, where after the pumps were throttled to keep a total pressure of 0.71 Pa for all depositions.

The choice of substrates and seed layers is essential in order to avoid peak overlaps in x-ray diffraction while keeping the lattice mismatch small and avoiding interdiffusion between layers. The lattice mismatch between the MgO substrate and ScN seed layer is 6.8%, leading to a clear peak separation in x-ray diffraction. Adding Al in the film leads to $Sc_{1-x}Al_xN$ peaks between ScN and MgO, with reduced crystalline quality for higher x. The Al molar fraction was chosen to ~0.4, which yields diffraction peaks easily separable from MgO and ScN while the value is also relatively close to $x=0.5$ used in $Ti_{1-x}Al_xN$. Here, the lattice-parameter difference between rocksalt TiN and AlN is less than 4%, and between TiN and MgO even only 0.7%, leading to peak overlap. Therefore, for the $Ti_{0.51}Al_{0.49}N$ films, $Al_2O_3(0001)$ substrates and no seed layers were used.

After the depositions, Ar and N_2 sputtering gases were removed and the as-deposited samples were stepwise annealed in vacuum (50–100 °C per step) to a maximum temperature of 1100 °C, with ramping times of less than 1 min. The temperature was kept constant and further x-ray diffraction scans were recorded until no phase changes in the films were observed. The dwell time at each temperature was always at least ~30 min but could reach a few hours for certain temperatures.

X-ray measurements were performed *in situ* using monochromatic synchrotron radiation with a wavelength of 1.05 Å. X-ray reflectivity measurements were performed to determine the thickness of the layers. After each deposition and in between each annealing step, symmetric $\theta/2\theta$ XRD scans were taken to follow the epitaxial growth and to check for possible phase changes. Pole figures of the annealed samples were recorded *ex situ* with the same wavelength on the same goniometer, using an Eulerian cradle. The measurements were performed in 3° steps with $0° \leq \varphi \leq 360°$ and $0° \leq \Psi \leq 90°$.

Rutherford backscattering spectroscopy (RBS), using a 2.0 MeV $^4He^+$ beam with an incidence angle of 55°, an scattering angle of 172° and evaluated with the SIMNRA code,[22] was performed *ex situ* to determine the film composition of as-deposited and annealed samples, and to check for eventual interdiffusion during annealing. Time-of-flight elastic recoil detection analysis (ERDA), using a 40 MeV $^{127}I^{9+}$ beam at 67.5° incidence and 45° recoil scattering angle and evaluated with the CONTES code,[23] was used in addition to determine the composition and to check for light elements and impurities in the films. Cross-sectional (scanning) transmission electron microscopy [(S)TEM] was carried out on a Tecnai G2 TF 20 UT FEG microscope operated at 200 kV. STEM energy-dispersive x-ray spectroscopy (EDX) maps of 45×25 nm^2 areas were obtained with 1 nm^2 pixel size. X-ray photoelectron spectroscopy (XPS) measurements were carried in a PHI Quantum 2000 instrument using Al $K\alpha$ radiation.

To shed further light on the studied topic, first-principles calculations within a density-functional theory approach were performed for the pseudobinary rocksalt alloys $Sc_{0.625}Al_{0.375}N$, $Sc_{0.50}Al_{0.50}N$, and $Ti_{0.50}Al_{0.50}N$ as well as for TiN, ScN, and c-AlN. The projector-augmented wave method as implemented in the Vienna *ab initio* simulation package[24–26] was used in combination with the generalized gradient approximation for exchange-correlation effects.[27] The alloys were modeled with the special quasirandom structure methods suggested by Zunger *et al.*[28] and further developed for pseudobinaries in the rocksalt structure by Alling *et al.*[13] k-point sampling of the Brillouine zone was performed using a Monkhorst-Pack scheme with a grid of $7 \times 7 \times 7$ points for the 64- and 48-atom supercells and with a $21 \times 21 \times 21$ grid for the TiN, ScN, and c-AlN binaries. An energy cutoff of 400 eV was used in the expansion of the wave functions.

III. RESULTS AND DISCUSSION

RBS shows that all as-deposited and annealed films have a stoichiometric (50 at. %) metal sublattice to within ±5 at. %. The remaining content is mainly nitrogen but

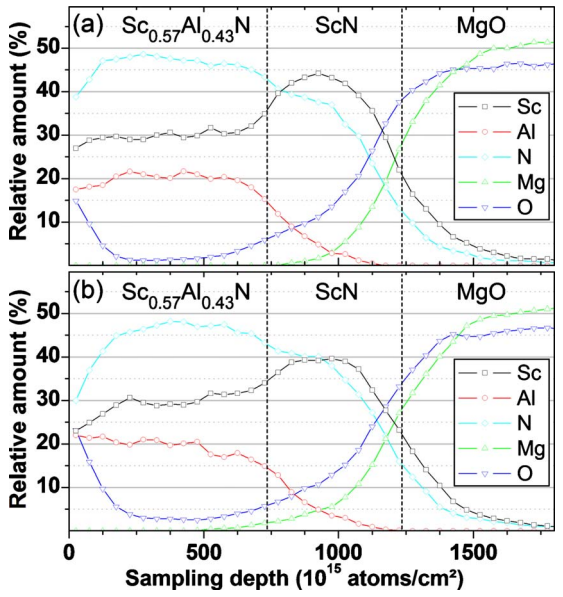

FIG. 1. (Color online) ERDA depth profiles from a $Sc_{0.57}Al_{0.43}N$ film grown on MgO(111) with a ScN(111) seed layer in (a) as-deposited and (b) annealed (1100 °C) states.

O, C, and H also exist in the film, further quantified with ERDA (see below). With the metal-to-N ratio set to 1, the resulting film compositions are $Sc_{0.57\pm0.02}Al_{0.43\pm0.02}N$ and $Ti_{0.51\pm0.02}Al_{0.49\pm0.02}N$. After annealing to temperatures of 1100 °C, no significant change in composition is seen for $Sc_{0.57}Al_{0.43}N$. After annealing $Ti_{0.51}Al_{0.49}N$ to 1066 °C, the amount of Al decreases relative to Ti throughout the film. The well-defined edges of all RBS peaks indicate that there has been no interdiffusion between substrates (seed layers) and films during deposition or annealing. All films with Sc contain up to 0.05 at. % Ta, which is a well-known contaminant in Sc sputter target material.

Figure 1 shows ERDA depth profiles from $Sc_{0.57}Al_{0.43}N$ films, including ScN seed layers and MgO substrates. The ERDA technique is more suitable for determining concentrations of light elements than RBS but the depth resolution is superior in RBS for films with thicknesses like the ones in this series. Therefore, a combination of these techniques was employed here. The ERDA depth profile from an as-deposited $Sc_{0.57}Al_{0.43}N$ film is shown in Fig. 1(a). The oxygen content is below 2 at. % in the film but higher close to the surface. The nitrogen content follows the oxygen almost perfectly so that they sum up to the 50 at. % required for stoichiometric nitrides, and we therefore assume that oxygen exists as a solid solution on the nitrogen sublattice. The Sc-to-Al ratio agreed well with the RBS results (not shown). The ERDA depth profile from a similar sample annealed to 1100 °C is shown in Fig. 1(b). Its compositional depth profile is very similar to the as-deposited case [cf. Fig. 1(a)]. The only significant difference is the slightly higher oxygen content throughout the annealed film. The similarity between the results from the as-deposited and annealed samples is of great importance for this study. It means that all phase transformations during annealing take place within the films, without influence from seed layers or substrates, and without loss of material to the vacuum.

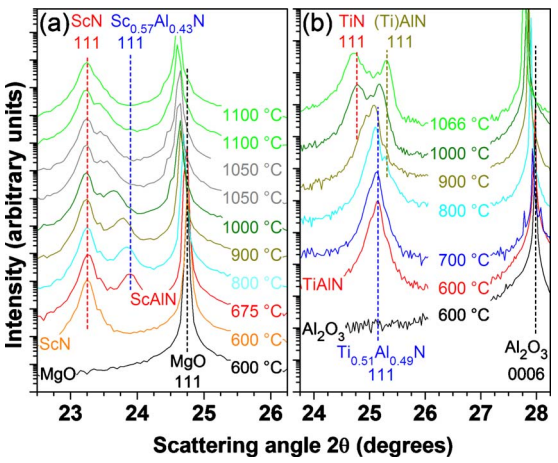

FIG. 2. (Color online) *In situ* XRD data of growth and annealing of epitaxial (a) ScN(111) seed layer (yellow) and $Sc_{0.57}Al_{0.43}N(111)$ film (red) onto MgO(111) and (b) $Ti_{0.51}Al_{0.49}N(111)$ film (red) onto $Al_2O_3(0001)$, recorded after growth of each layer and stabilization of each annealing temperature.

An ERDA depth profile from $Ti_{0.51}Al_{0.49}N$ (not shown) showed an amount of ~16 at. % oxygen in the as-deposited film, again with oxygen probably positioned on the nitrogen sublattice. After annealing to 1066 °C, there are noticeable compositional variations in the film, with global concentrations of $Ti_{0.35}Al_{0.10}N_{0.35}O_{0.18}$ close to the surface and $Ti_{0.22}Al_{0.23}N_{0.20}O_{0.34}$ next to the substrate interface. It seems that a substantial loss of Al into the vacuum chamber has occurred, simultaneous with O uptake by inward diffusion from the ambient. A similar behavior has been observed in Ref. 29 when synthesizing nitrogen understoichiometric Ti-Al-N films at 675 °C. XPS measurements on the annealed sample indicate that oxygen is bonded both as Al_2O_3 and TiO_2. Furthermore, the concentration of other impurities, such as C and H in all films are close to the detection limit of ~0.1 at. % in ERDA.

Figure 2 shows *in situ* XRD scans recorded during deposition and annealing of (a) a $Sc_{0.57}Al_{0.43}N$ (111) film and ScN(111) seed layer, which are deposited onto MgO(111) at 675 °C and 600 °C, respectively, and (b) a $Ti_{0.51}Al_{0.49}N$ film, which is deposited onto $Al_2O_3(0001)$ at 600 °C. For the $Sc_{0.57}Al_{0.43}N$ case, no phase change is observed up to 900 °C. The film peak slightly shifts to lower angles when increasing the temperature. Repeated scans every 30 min at constant temperature do not change the shape of the diffractogram, meaning that the shift of the peak is only due to thermal expansion of the crystal lattice. When increasing the temperature to 1000 °C, the shift of the $Sc_{0.57}Al_{0.43}N$ 111 peak toward lower angle is more pronounced and continues for a repeated scan 30 min later. Still, the process is very slow and would need several hours for a complete overlap with the peak from the ScN(111) seed layer. In fact, an increase in temperature to 1050 and 1100 °C leads to a distinguishable peak shift between individual 30 min scans. After ~1 h at 1100 °C, the film peak has completely vanished. No additional peaks appear in large-angle overview scans. In combination with the RBS and ERDA results, this implies that stoichiometric $Sc_{0.57}Al_{0.43}N(111)$ has completely de-

composed into c-ScN(111) and AlN with a retained global composition (x=0.43).

For the case of $Ti_{0.51}Al_{0.49}N$, Fig. 2(b) shows that during annealing the film peak slightly broadens at 800 and 900 °C, with two small shoulders emerging at higher and lower angles. This is in agreement with the initial steps of spinodal decomposition, where c-AlN and TiN-rich domains form. The results are similar to a previous *ex situ* study of films with a similar composition.[6] We thus observe that the first sign of spinodal decomposition in our study agrees with the so-called DSC2 peak at ~800 °C in Fig. 2 in Ref. 6. It is not until 1000 °C that the film in the present experiment clearly phase separates into TiN(111) and c-AlN(111), which is in line with DSC3 in the same reference. The resulting TiN lattice parameter is 4.25 Å, which deviates by only 0.01 Å from literature values.[30] The deviation of the measured lattice-parameter value for c-AlN of a=4.15 Å, is, however, slightly higher than literature values ranging from a =4.05–4.12 Å (Refs. 31 and 32) (ICDD PDF 25-1495). There are three possible explanations for that: (1) stressed c-AlN domains to maintain coherency to the matrix, (2) residual TiN in the AlN lattice, and (3) thermal expansion.

We conclude that the present results are similar to those reported in previous experimental studies performed on phase separation of c-$Ti_{0.50}Al_{0.50}N$.[6] Furthermore, our results show that the phase-separation process occurs in qualitatively different ways for $Sc_{1-x}Al_xN$ and $Ti_{1-x}Al_xN$, as no residual c-AlN is visible in the $Sc_{1-x}Al_xN$ XRD measurements.

Cross-sectional transmission electron microscopy images were taken from three different $Sc_{0.57}Al_{0.43}N$ films, in the as-deposited state, and after annealing to 1000 °C and 1100 °C, respectively. Overview images showed that the films and seed layers have a columnar microstructure with low-energy surface facets. This is typical for transition-metal nitride growth far from thermal equilibrium, and with low ion bombardment on high-energy surfaces.[33] Likewise, there is also no significant difference in the morphology between as-deposited and annealed samples, due to the lack of bulk diffusion, and the images are similar to Fig. 4(a) in Ref. 16.

In order to probe deeper into the phase separation during annealing, EDX maps were recorded for the three samples which are shown in Figs. 3(a)–3(c). The green (light) color corresponds to Sc-rich and the blue (dark) color to Al-rich regions in the film. In the as-deposited sample in Fig. 3(a), the Sc and Al atoms are nearly evenly distributed throughout the film, as expected from the XRD results above (cf. Fig. 2), and thus corroborate the conclusion of a solid solution of $Sc_{0.57}Al_{0.43}N$. Figure 3(b) reveals that both Sc- and Al-rich regions have started to form in the sample that was annealed to 1000 °C for 1 h. This is in agreement with the observed shift of the $Sc_{0.57}Al_{0.43}N$ 111 peak toward ScN 111 in XRD. After annealing at 1100 °C for 1.5 h, a near complete phase transformation of $Sc_{0.57}Al_{0.43}N$ into ScN and AlN can be seen in Fig. 3(c). The Sc-rich and Al-rich domains in the sample are almost perpendicular to the seed layer, only a few nanometer wide and elongated with a length that reaches throughout the whole film thickness, based on Z-contrast images obtained by STEM. Any compositional fluctuations [not discernable in Fig. 3(a)] along domain boundaries that

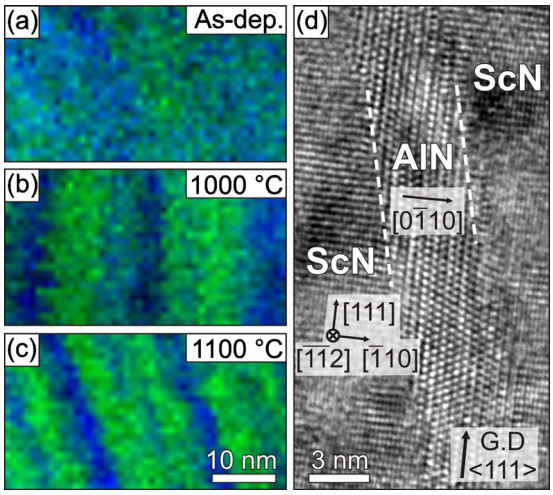

FIG. 3. (Color online) Cross-sectional transmission electron microscopy images showing (a)–(c) EDX maps with Sc-rich (green) and Al-rich (blue) regions of (a) the as-deposited, (b) 1000 °C annealed, and (c) 1100 °C annealed $Sc_{0.57}Al_{0.43}N$ films, together with (d) a lattice-resolved image from the same film annealed at 1100 °C with indexing of AlN and ScN domains.

formed during growth of $Sc_{0.57}Al_{0.43}N$ likely assist the nucleation of w-AlN.

To determine the overall orientation of the AlN domains in relation to the surrounding c-ScN, pole figures are recorded from the 1100 °C annealed sample. Figures 4(a) and 4(b) present {$\bar{1}$100} and {0002} pole figures of w-AlN, respectively, assuming literature values of w-AlN lattice parameters a=3.11 Å and c=4.98 Å.[34]

The {$\bar{1}$100} pole figure in Fig. 4(a) reveals three clusters of intensity from ($\bar{1}$100) and ($\bar{1}$010) at $\Psi \sim 45°$, which are separated by ~120° in φ, corresponding to a threefold symmetry of w-AlN. The clusters are indexed with blue squares, triangles, and rings, respectively. The three reflections visible at $\Psi \sim 70°$, separated by ~120° in φ, together with the reflection in the center correspond to ScN {111} planes, show up due to a slight overlap between the ScN 111 and AlN $\bar{1}$100 peaks. ScN in the annealed film has the same threefold symmetry as as-deposited $Sc_{0.57}Al_{0.43}N$, and this orientation is originally due to the epitaxial growth onto the underlying ScN(111) seed layer.

In Fig. 4(b), the pole figure of the {0001} planes of w-AlN reveals three distinct orientations, as a consequence of the threefold texture symmetry of the w-AlN crystallites. The reflections are indexed corresponding to Fig. 4(a). MgO 111 reflections are seen in this pole figure due to the small difference in plane spacing of w-AlN(0001) and MgO(111), yielding a partial overlap in XRD.

Figure 4(c) shows a schematic stereographic projection of all w-AlN poles visible in the pole figures (indexed in blue according to the three symbols mentioned above) together with the angular positions of the {111} and certain {110} poles from ScN (indexed with green crosses). For w-AlN, only the ring-shaped symbols are indexed but the squares and triangles can easily be indexed by a clockwise rotation around the origin of 120° and 240°, respectively. We

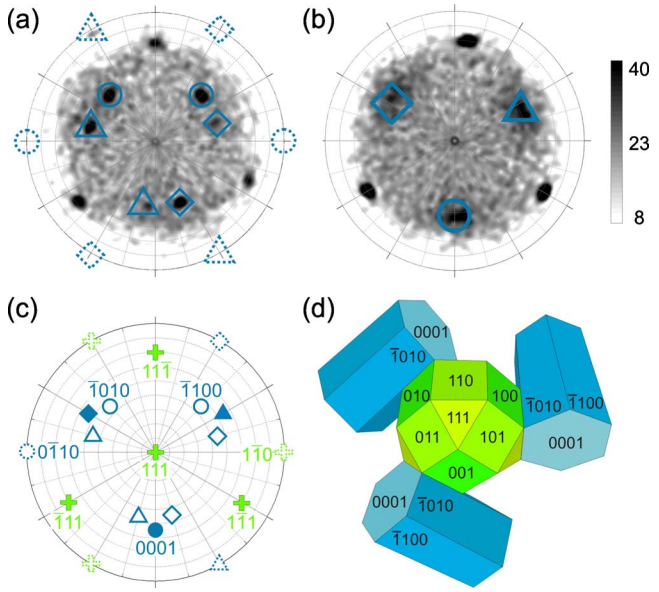

FIG. 4. (Color online) Pole figures from the $Sc_{0.57}Al_{0.43}N(111)$ sample annealed at 1100 °C showing (a) $\{\bar{1}100\}$ and (b) {0002} poles from w-AlN, exhibiting a threefold symmetry of w-AlN, with each associated orientation labeled with blue squares, triangles, and rings, respectively. The stereographic projection in (c) shows the topotaxial relations between w-AlN [labeled as in (a) and (b)] and ScN (green crosses). For readability, only rings and crosses are indexed. (d) illustrates the topotaxial relations between c-ScN (green) and three (out of six) possible orientations of w-AlN (blue).

note that only two of the in total six permutations of w-AlN$\{\bar{1}100\}$ can be seen in the pole figure in Fig. 4(a). Two more permutations would be at $\Psi=90°$ and $\varphi=90°$ or 270° but these angles cannot be reached with the used experimental setup and are therefore marked with dotted symbols in Figs. 4(a) and 4(c). From the stereographic projection, we can thus conclude that w-AlN$\langle 0\bar{1}10\rangle \| $c-ScN$\langle\bar{1}10\rangle$. The w-AlN 0001 reflections are indexed with solid symbols. They have an exact angular overlap with the three 001 reflections of ScN (not shown), meaning that ScN(001)$\|$w-AlN(0001).

A schematic illustration of the topotaxial relations between c-ScN and w-AlN in the phase separated film is shown in Fig. 4(d). The c-ScN is drawn in green (light gray in black and white contrast), with the [111] growth direction perpendicular to the paper plane. Hexagons that represent w-AlN are drawn in blue (dark gray) for three out of the six ScN {110} permutations of planes, which are perpendicular to ScN(111). It can be seen that w-AlN(0001)$\|$ScN(001) and w-AlN$\langle 0\bar{1}10\rangle \|$c-ScN$\langle\bar{1}10\rangle$. The resulting lattice mismatch along w-AlN$\langle 1\bar{2}10\rangle \|$c-ScN$\langle\bar{1}\bar{1}0\rangle$ is −2.5% and the mismatch along ScN$\langle 001\rangle \|$w-AlN$\langle 0001\rangle$ is +10.4%.

A lattice-resolved TEM image from the 1100 °C annealed sample in Fig. 3(d) shows that ScN and w-AlN domains form coherently from the original c-$Sc_{0.57}Al_{0.43}N(111)$. The orientation of an individual AlN domain in relation to the surrounding ScN is illustrated in the image and agrees with the general topotaxial relations obtained from the $\{\bar{1}100\}$ and {0002} pole figures in Figs. 4(a) and 4(b).

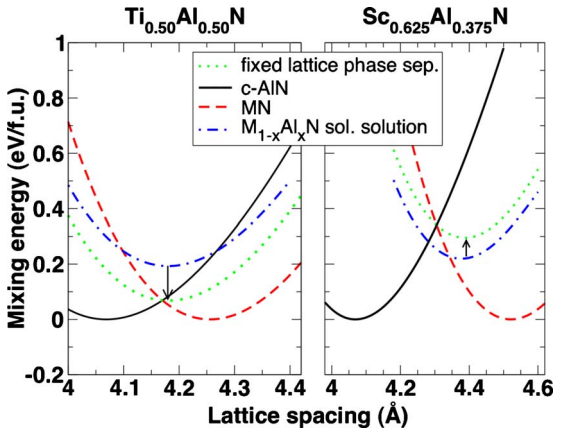

FIG. 5. (Color online) Calculated and normalized energy-lattice spacing curves for $Ti_{0.50}Al_{0.50}N$ (left) and $Sc_{0.625}Al_{0.375}N$ (right). The curves of the solid solutions are shown with blue dashed-dotted lines while the green dotted lines show hypothetical phase separations, for which the resulting lattice spacing is forced to be the same for both components. The qualitative difference between the systems in an isostructural coherent situation is indicated by black arrows.

Our experimental investigation of the phase-separation process in c-$Sc_{1-x}Al_xN$ and c-$Ti_{1-x}Al_xN$ solid solutions demonstrates a qualitatively different behavior in the two systems. While our results confirm the operation of spinodal decomposition in c-$Ti_{1-x}Al_xN$, c-$Sc_{1-x}Al_xN$ transforms by nucleation and growth of w-AlN. To understand why the c-$Sc_{1-x}Al_xN$ system does not decompose in an isostructural way, meaning that there are no signs of c-AlN in the Sc-containing system or why $Ti_{1-x}Al_xN$ does not decompose to ground-state w-AlN directly, it is necessary to consider the driving forces for phase separation.

For that purpose, we have performed first-principles calculations of the mixing energy-lattice spacing curves for $Sc_{0.625}Al_{0.375}N$, $Sc_{0.50}Al_{0.50}N$, and $Ti_{0.50}Al_{0.50}N$ cubic solid solutions as well as the binary ScN, TiN, and c-AlN phases. Figure 5 shows the calculated energy versus lattice spacing curves of $Ti_{0.50}Al_{0.50}N$ (left) and $Sc_{0.625}Al_{0.375}N$ (right). Results for $Sc_{0.50}Al_{0.50}N$ can be found in Ref. 35, which are very similar to that of our $Sc_{0.625}Al_{0.375}N$. c-AlN is shown with a black solid line and has an energy minimum at the calculated lattice spacing of 4.068 Å. The TiN and ScN curves are drawn with dashed red lines, yielding lattice spacings of 4.255 Å and 4.521 Å, respectively. All calculated lattice parameters are in good agreement with reported experimental values. The energies of the binary phases are normalized to zero. The energy-lattice spacing curves of the ternary solid solutions are shown with blue dashed-dotted lines, with the energies normalized to the mixing energies according to $E_{mix}=E(M_{1-x}Al_xN)-(1-x)\times E(MN)-x\times E(\text{c-AlN})$. The energy-lattice spacing curves that are drawn in green dotted lines show the mixing energies for a hypothetical phase-separation case, where the resulting *MN* and c-AlN components are forced to have the same lattice spacing. A qualitative difference between the $Sc_{1-x}Al_xN$ and $Ti_{1-x}Al_xN$ systems is directly seen when comparing the driving forces for phase separation if the resulting *MN* and

c-AlN components are required to have the same lattice spacing. In the $Ti_{1-x}Al_xN$ system, the solid solution has a strong driving force for isostructural phase separation even in situations where the resulting phases cannot relax their volumes. The reason for this is a strong electronic-structure mismatch effect, which is described in Ref. 13. In $Sc_{1-x}Al_xN$, on the other hand, this effect is absent since Sc and Al have the same valence.[19] Indeed, there is no driving force for fixed lattice decomposition in $Sc_{0.625}Al_{0.375}N$, as the energy for that is higher as compared to the solid solution for all lattice spacings. This means, that in order for isostructural phase separation to occur in $Sc_{1-x}Al_xN$, the resulting cubic phases must be allowed to have a considerable amount of volume relaxation. This is, however, not possible during the initial stages of spinodal decomposition.

Instead of isostructural phase separation, one could expect the existence of an isostructural *ordering* tendency of Sc and Al atoms, similar to the observed bulk coherency in theoretically studied zinc-blende structure $Ga_{1-x}In_xN$.[36] However, in that study, the ordering temperatures were found to be very much lower than the critical temperature for volume relaxed phase separation, and thus we believe that our as-deposited $Sc_{1-x}Al_xN$ films are indeed solid solutions. The supersaturated solid solution of $Sc_{0.625}Al_{0.375}N$ can however serve as an AlN donor since it is not trapped into a metastable isostructural decomposing state. At high enough temperatures, however, the diffusion is sufficient for nucleation and growth type phase separation at the domain boundaries. The relatively small lattice mismatch between ScN($\bar{1}$10) and w-AlN(0$\bar{1}$10) enables phase transformation by the formation of c-ScN and w-AlN with semicoherent interfaces, which from pole figures and lattice-resolved TEM was seen to occur. As the formation of AlN takes place through nucleation and growth, the observed formation of ground-state w-AlN rather than c-AlN is what should be expected from the considerably higher energy of the latter.

Our work proves the importance of understanding the physics of thin-film materials on the most fundamental level if distinct and better performing materials, particularly metastable pseudobinary phases, are to be found. We show experimentally that the particular *driving force* for phase separation, i.e., electronic-structure or volume mismatch, rather than the amplitude of the positive mixing enthalpy decides the decomposition path and resulting morphology of heat treated thin films. c-$Ti_{1-x}Al_xN$ undergoes spinodal decomposition into coherent isostructural AlN and TiN at high temperatures while c-$Sc_{1-x}Al_xN$ phase separates through nonisostructural nucleation and growth of coherent w-AlN at the domain boundaries of a c-ScN matrix, initiated first at even higher temperatures. The impact of the spinodal decomposition on the hardness and cutting performance of $Ti_{1-x}Al_xN$ coatings is well known while the effect of the process at work in $Sc_{1-x}Al_xN$ films remains to be investigated.

IV. CONCLUSIONS

We have shown by thin-film deposition and stepwise annealing that volume and electronic-structure mismatch as the driving forces for phase separation give rise to qualitatively different decomposition behavior and resulting morphology in the metastable rocksalt c-$Sc_{1-x}Al_xN$ and c-$Ti_{1-x}Al_xN$ solid solutions, respectively. Reactive magnetron sputter-deposited $Sc_{0.57}Al_{0.43}N(111)$ films phase separate at 1000–1100 °C, by nucleation and growth at the domain boundaries into coherent c-ScN and w-AlN due to volume mismatch of the respective cubic binaries. The topotaxial relationship is AlN(0001)$\|$ScN(001) and AlN$\langle 0\bar{1}10\rangle\|ScN\langle\bar{1}10\rangle$. This is in contrast to $Ti_{0.51}Al_{0.49}N(111)$ that undergoes spinodal decomposition into isostructural and coherent TiN and AlN already at 800–1000 °C primarily because of the system's electronic structure. First-principles calculations of mixing energy-lattice spacing curves explain the results and open a route for design of novel metastable pseudobinary phases based on an understanding of the physics of functional materials systems on the most fundamental level.

ACKNOWLEDGMENTS

The authors acknowledge Luc Orthega at CNRS, Grenoble, for letting us use the x-ray diffractometers at an initial stage, the Tandem Laboratory at Uppsala University for giving us access to the ion-beam facilities, and Andrej Furlan at Uppsala University for performing XPS measurements. Financial support was given by the Swedish Research Council (VR), The European Research Commission (ERC), and the Swedish Foundation for Strategic Research (SSF). The calculations were performed at the Swedish National Supercomputer Centre (NSC) using resources provided by the Swedish National Infrastructure for Computing (SNIC).

[1] O. Knotek, W. D. Münz, and T. Leyendecker, J. Vac. Sci. Technol. A **5**, 2173 (1987).
[2] K. Bobzin, E. Lugscheider, R. Nickel, and P. Immich, Materialwiss. Werkstofftech. **37**, 833 (2006).
[3] K. Kutschej, P. H. Mayrhofer, M. Kathrein, P. Polcik, R. Tessadri, and C. Mitterer, Surf. Coat. Technol. **200**, 2358 (2005).
[4] W.-D. Münz, J. Vac. Sci. Technol. A **4**, 2717 (1986).
[5] D. McIntyre, J. E. Greene, G. Håkansson, J.-E. Sundgren, and W.-D. Münz, J. Appl. Phys. **67**, 1542 (1990).
[6] P. H. Mayrhofer, A. Hörling, L. Karlsson, J. Sjölén, C. Mitterer, and L. Hultman, Appl. Phys. Lett. **83**, 2049 (2003).
[7] D. J. Seol, S. Y. Hu, Y. L. Li, J. Shen, K. H. Oh, and L. Q. Chen, Acta Mater. **51**, 5173 (2003).
[8] J. W. Cahn, Trans. Metall. Soc. AIME **242**, 166 (1968).
[9] *Phase Transformations in Metals and Alloys*, 2nd ed., edited by D. A. Porter and K. E. Easterling (Taylor & Francis, Boca Raton, FL, 2004).
[10] L. Karlsson, A. Hörling, M. P. Johansson, L. Hultman, and G. Ramanath, Acta Mater. **50**, 5103 (2002).
[11] F. Adibi, I. Petrov, L. Hultman, U. Wahlström, T. Shimizu, D.

McIntyre, J. E. Greene, and J.-E. Sundgren, J. Appl. Phys. **69**, 6437 (1991).
[12] A. Hörling, L. Hultman, M. Odén, J. Sjölén, and L. Karlsson, J. Vac. Sci. Technol. A **20**, 1815 (2002).
[13] B. Alling, A. V. Ruban, A. Karimi, O. E. Peil, S. I. Simak, L. Hultman, and I. A. Abrikosov, Phys. Rev. B **75**, 045123 (2007).
[14] J. C. Schuster and J. Bauer, J. Less-Common Met. **109**, 345 (1985).
[15] C. Höglund, J. Birch, M. Beckers, B. Alling, Zs. Czigány, A. Mücklich, and L. Hultman, Eur. J. Inorg. Chem. **2008**, 1193.
[16] C. Höglund, J. Bareno, J. Birch, B. Alling, Zs. Czigany, and L. Hultman, J. Appl. Phys. **105**, 113517 (2009).
[17] A. Kimura, H. Hasegawa, K. Yamada, and T. Suzuki, Surf. Coat. Technol. **120-121**, 438 (1999).
[18] M. Zhou, Y. Makino, M. Noose, and K. Nogi, Thin Solid Films **339**, 203 (1999).
[19] B. Alling, A. Karimi, and I. A. Abrikosov, Surf. Coat. Technol. **203**, 883 (2008).
[20] F. Rovere, D. Music, S. Ershov, M. Baben, H.-G. Fuss, P. H. Mayrhofer, and J. M. Schneider, J. Phys. D: Appl. Phys. **43**, 035302 (2010).
[21] N. Schell, J. v. Borany, and J. Hauser, AIP Conf. Proc. No. 879 (AIP, New York, 2007), p. 1813.
[22] www.simnra.com
[23] M. S. Janson, CONTES—conversion of time-energy spectra—a program for ERDA data analysis, internal report, Uppsala University, 2004.
[24] P. E. Blöchl, Phys. Rev. B **50**, 17953 (1994).
[25] G. Kresse and J. Hafner, Phys. Rev. B **48**, 13115 (1993).
[26] G. Kresse and J. Hafner, Phys. Rev. B **49**, 14251 (1994).
[27] J. Perdew, K. Burke, and M. Ernzerhof, Phys. Rev. Lett. **77**, 3865 (1996).
[28] A. Zunger, S. H. Wei, L. G. Ferreira, and J. E. Bernard, Phys. Rev. Lett. **65**, 353 (1990).
[29] M. Beckers, C. Höglund, C. Baehtz, R. M. S. Martins, P. O. Å. Persson, L. Hultman, and W. Möller, J. Appl. Phys. **106**, 064915 (2009).
[30] J.-E. Sundgren, Thin Solid Films **128**, 21 (1985).
[31] H. Vollstädt, E. Ito, M. Akaishi, S. Akimoto, and O. Fukunaga, Proc. Jpn. Acad., Ser. B: Phys. Biol. Sci. **66**, 7 (1990).
[32] A. Madan, I. W. Kim, S. C. Cheng, P. Yashar, V. P. Dravid, and S. A. Barnett, Phys. Rev. Lett. **78**, 1743 (1997).
[33] I. Petrov, P. B. Barna, L. Hultman, and J. E. Greene, J. Vac. Sci. Technol. A **21**, S117 (2003).
[34] H. Schulz and K. Thiemann, Solid State Commun. **23**, 815 (1977).
[35] B. Alling, Ph.D. dissertation, École Polytechnique Fédérale de Lausanne, 2009.
[36] J. Z. Liu and A. Zunger, Phys. Rev. B **77**, 205201 (2008).